JOURNAL OF EXTRACELLULAR VESICLES, 2017
VOL. 6, 1324730
https://doi.org/10.1080/20013078.2017.1324730

Taylor & Francis
Taylor & Francis Group

RESEARCH ARTICLE

OPEN ACCESS Check for updates

Comprehensive toxicity and immunogenicity studies reveal minimal effects in mice following sustained dosing of extracellular vesicles derived from HEK293T cells

Xiaohua Zhu[a], Mohamed Badawi[a], Steven Pomeroy[b], Dhruvitkumar S. Sutaria[a], Zhiliang Xie[a], Alice Baek[a], Jinmai Jiang[b], Ola A. Elgamal[a], Xiaokui Mo[c], Krista La Perle[d], Jeffrey Chalmers[e], Thomas D. Schmittgen[b] and Mitch A. Phelps[a]

[a]College of Pharmacy, The Ohio State University, Columbus, OH, USA; [b]College of Pharmacy, University of Florida, Gainesville, FL, USA; [c]Department of Biostatistics, The Ohio State University, Columbus, OH, USA; [d]College of Veterinary Medicine, The Ohio State University, Columbus, OH, USA; [e]College of Engineering, The Ohio State University, Columbus, OH, USA

ABSTRACT

Extracellular vesicles (EVs) are under evaluation as therapeutics or as vehicles for drug delivery. Preclinical studies of EVs often use mice or other animal models to assess efficacy and disposition. However, as most EVs under evaluation are derived from human cells, they may elicit immune responses which may contribute to toxicities or enhanced EV clearance. Furthermore, EVs from different cell sources or EVs comprising various cargo may differ with respect to immunogenicity or toxicity. To assess EV-induced immune response and toxicity, we dosed C57BL/6 mice with EVs intravenously and intraperitoneally for 3 weeks. EVs were harvested from wild type or engineered HEK293T cells which were modified to produce EVs loaded with miR-199a-3p and chimeric proteins. Blood was collected to assess hematology, blood chemistry, and immune markers. Spleen cells were immunophenotyped, and tissues were harvested for gross necropsy and histopathological examination. No signs of toxicity were observed, and minimal evidence of changes in immune markers were noted in mice dosed with engineered, but not with wild type EVs. This study provides a framework for assessment of immunogenicity and toxicity that will be required as EVs from varying cell sources are tested within numerous animal models and eventually in humans.

ARTICLE HISTORY
Received 22 December 2016

RESPONSIBLE EDITOR
Raymond Michel Schiffelers
NETHERLANDS

KEYWORDS
Exosomes; drug carriers; C57BL/6; miR-199a-3p; cytokines; immunophenotyping; immunogenicity; toxicity

Introduction

Exosomes are small membrane vesicles (40–100 nm) that originate from early endosomes and are secreted by most cell types as one form of extracellular vesicle (EV) upon fusion of late endosomes with the plasma membrane [1,2]. They contain a variety of cellular contents such as proteins, messenger RNA (mRNA), and microRNA (miRNA) which can be functionally exchanged between cells [3,4]. The natural ability of exosomes to transfer these biological materials between cells and subsequently to modulate biological processes in the recipient cells, together with recent advances in isolation and purification of these small particles [5,6], demonstrate their potential as delivery vessels for genetic material, proteins, or even small molecules [1,7]. Several studies exploiting exosomes or EVs as drug-delivery systems have been conducted to deliver therapeutic miRNAs, and the results have shown that exosomes successfully deliver functional miRNAs to the targeted cells both *in vitro* and *in vivo* and demonstrate favourable biological activity and efficacy, indicating their promise as a new class of drug-delivery vehicles [8–12].

While demonstration of efficacy is important in early preclinical development, identifying toxicities and deciphering their causes is equally critical for experimental therapies. Although extensive studies have been conducted to evaluate the immune-regulatory role of EVs derived from different immune cells such as B cells, T cells, dendritic cells (DCs), and macrophages [13–19], little is known about the broader potential for immunogenic or toxic effects of EVs. This is especially important given that therapeutic EVs, which are most often derived from human cell lines, will be tested in rodents and various other animal disease models throughout preclinical development. As with other biological therapeutics such as monoclonal antibodies and cell-based therapies which may induce toxicity secondary to immune response or as a primary on- or off-target effect [20–22], care must be taken to ensure that we have a thorough understanding of the immunogenic or toxic potential of therapeutic EVs.

CONTACT Mitch A. Phelps phelps.32@osu.edu College of Pharmacy, The Ohio State University, 500 West 12th Avenue, Columbus, OH 43210, USA
Supplemental data for this article can be accessed here.

The immunogenicity and toxicity of EVs depend both on the animal models used in testing and on the source and composition of the EVs. Although some argue that immortalised cells should not be used for production of therapeutic EVs since some of the EV cargo may carry toxic or even carcinogenic constituents [23–25], different immortalised cell lines have been used commonly as EV producers owing to the infinite supply of cells for EV production, increased proliferative rate, and the ease of genetically modifying these cells [26,27]. The human embryonic kidney cell line HEK293T has been used to produce EVs for a broad array of studies, in part owing to its capacity for high yield of EVs, ease of growth, and high transfection efficiency [28–31].

In our efforts to develop therapeutic EVs, we have engineered HEK293T cells to produce miR-199a-3p-loaded vesicles. miR-199a-3p was shown to reduce proliferation in CD44-positive hepatocellular carcinoma (HCC) cells [32]. We incorporated within a chimeric protein a FLAG peptide (as a tag for vesicle isolation), the phage clone PC94 (a peptide that specifically binds to HCC cells [33,34]), lysosome-associated membrane protein-2a (Lamp2a, a protein enabling abundant targeting of the chimera into EV membranes [35]), transactivator of transcription (TAT) peptide [a human immunodeficiency virus-1 (HIV-1) transactivator protein that binds to transactivation response (TAR) element RNA], and the polyhistidine tag 6xHIS (as a tag for chimeric protein detection). We also engineered within an intron of our chimeric protein, pre-miR-199a-3p, with a modified loop containing the TAR RNA sequence (therapeutic miR), thus enabling the TAT–TAR interaction to enhance loading of the pre-miR-199a-3p into the engineered HEK293T EVs. A complete description of the engineered EVs from the HEK293T is described in a separate study [36]. We previously demonstrated that EVs were efficiently internalised by human monocytic cells without causing a cytotoxic effect or altering phagocytic efficiency on the cell lines evaluated [37]. Given that EVs derived from human cell lines are under evaluation as carriers for therapeutic agents, and ongoing studies often use mouse disease models for evaluation of disposition, activity, or efficacy, and also since there is general concern over using human immortalised cell lines as EV producers owing to the tumorigenic potential or toxic potential of the EVs, it is imperative that we determine the potential for immunogenic and toxic effects of these EVs in mice. The aim of the current study was therefore to thoroughly assess the potential of wild-type (WT) or engineered HEK293T cell-derived EVs to induce toxicity and immune responses in mice. This was achieved by evaluating cytokine levels, spleen immune cell composition, and general toxicity after mice received 3 weeks of dosing with the EVs.

Materials and methods

Cell lines

Wild-type HEK293T cells (WT, ATCC CRL-11268) were cultured in Dulbecco's modified Eagle's medium (DMEM) (Life Technologies, Carlsbad, CA, USA) supplemented with 5% foetal bovine serum (Sigma, St Louis, MO, USA) that was depleted of EVs by ultracentrifugation (110,000 × *g*, 18 h). HEK293T cells transfected with empty vector (Empty), the full chimeric construct without miR-199a-3p (Full no 199), and the full construct with miR-199a-3p (Full with 199) (Sutaria et al., [36]) were cultured in the above media with 75 μg/mL hygromycin.

EV isolation and characterisation

EVs were isolated via ultracentrifugation according to our previously published paper [37]. In brief, when the cells cultured in 150 mm tissue culture dishes (VWR, Radnor, PA, USA) reached 80–90% confluence (about 20 million cells/dish), conditioned medium was recovered from 24 dishes (about 20 mL/dish) for EV isolation. Collected medium was centrifuged at 300 × *g* for 10 min followed by 2000 × *g* for 20 min, and then 10,000 × *g* for 30 min. Supernatants were filtered using 0.22 μm filter units and ultracentrifuged at 110,000 × *g* for 75 min. EV pellets were washed with phosphate-buffered saline (PBS) twice and resuspended in PBS containing 1% dimethylsulfoxide (DMSO) to reduce vesicle aggregation and to avoid potential clumping of EVs as we prepared and injected concentrated dosing solutions (e.g. 8.5 μg EV proteins per 100 μl PBS). The EV resuspension was stored at −80°C after preparation of the samples for EV characterisation. The protein concentration was measured by the bicinchoninic acid assay (BCA) method. Cryo-transmission electron microscopy (Cryo-TEM) was used to study the morphology of the isolated EVs. The size distribution and number of EVs were determined using nanoparticle tracking analysis (NTA) on a Nanosight NS300 instrument (Malvern Instruments, Westborough, MA, USA). The presence of miR-199a-3p and 6xHIS protein in EVs isolated from engineered cells was confirmed by quantitative polymerase chain reaction (qPCR) and Western blot, respectively. Details of Cryo-TEM, NTA, and

Western blot methods are provided in the supplementary materials section.

Animal study and pathology

The animal study was performed in C57BL/6 mice following the protocols approved by the Institutional Animal Care and Use Committees (IACUCs) of The Ohio State University. Female, 6–7 week-old mice were purchased from Envigo (previously Harlan, Indianapolis, IN, USA) and housed in a barrier rodent facility with free access to standard chow diet and water for 1 week before the experiment. The protein concentration of EVs was adjusted to 85 μg/mL using PBS containing 1% DMSO before the experiment. Characterisation of EVs to confirm particle size, 6xHIS tag presence, and miR-199a-3p content is described in the supplemental materials section. Animals were randomly divided into five groups (n = 10/group) and received either PBS containing 1% DMSO, WT, Empty, Full no 199, or Full with 199 EVs at 8.5 μg protein/mouse/day (approximately 10^{10} EVs per dose, dose volume = 100 μL/mouse) three times a week, with the first dose administered intravenously (i.v.) by tail vein injection and the second and third doses administered by the intraperitoneal route. One final intraperitoneal dose was administered on day 22 after 3 weeks of dosing, and all the mice were killed on day 23, 1 day after the last dose was given (Supplementary Figure 1). Mice challenged with 0.4 mg/kg lipopolysaccharide (LPS) three times (0, 6, and 24 h) by the intraperitoneal route were included as a technical control, and mice receiving vehicle (0.9% saline) by the same route were included as a vehicle control to demonstrate that the various measurements we were making (e.g. Rodent MAP and immune cell phenotyping) were in fact identifying the anticipated signals from our LPS technical control group.

Animals were monitored during the entire study for visible signs of toxicity. Submandibular blood collection was performed before the first dose (day 1), 1 day after the first dose (day 3), and before the animals were killed (day 23) for complete blood count analysis (Hematology Analyzer FORCYTE Autosampler 10; Oxford Science, Oxford, CT, USA). Whole blood was collected by cardiac puncture following death, and serum was harvested upon centrifugation at 900 × g for 10 min at 4°C for biochemical profiling (VetAce Chemistry Analyzer; Alfa Wasserman, West Caldwell, NJ, USA) and the Rodent MAP test.

Complete post-mortem evaluations were performed on all mice, and body and organ (thymus, heart, lungs, liver, spleen, kidneys, adrenals, ovaries and uterus, and brain) weights were obtained for all mice. Portions of spleens were harvested for immunophenotyping analysis. All tissues were collected, separated into halves, and then flash frozen and fixed in 10% neutral buffered formalin. Following fixation, the skull, sternum, vertebral column, and rear leg from each mouse were decalcified in Decalcifier I (Surgipath Medical Industries, Richmond, IL, USA) for 48 h. After formalin fixation, all tissues were processed by routine methods and embedded in paraffin. Sections (4 μm) were stained with hematoxylin and eosin (HE) and evaluated by a veterinary pathologist certified by the American College of Veterinary Pathologists.

Rodent MAP

Serum was prepared from whole blood samples collected after death (as described above) following coagulation of whole blood at room temperature for 30 min. A portion of each serum sample (75 μL) was sent to Ampersand Biosciences (Saranac Lake, NY, USA) for analysis of 42 biomarkers on the Rodent MAP v.4.0 platform (Supplementary Table 1).

Spleen cell immunophenotyping

Splenocytes were isolated as described previously [38] and stained with surface biomarkers conjugated with different fluorochromes for flow cytometry immunophenotyping experiments. Surface markers for these experiments included the macrophage/monocyte/neutrophil marker CD11b-VioGreen; T-cell markers CD8a-VioBlue, CD3e-PE-Vio770, and CD4-APC; natural killer (NK) cell marker anti-NK1.1-PE; DC marker CD11c-FITC; and B-cell marker CD19-APC-Vio770 (Miltenyi Biotech, Cambridge, MA, USA). Cell counts were acquired on an LSR II cytometer (BD Immunocytometry Systems, San Jose, CA, USA). The viable, single cell population was gated based on forward scatter and side scatter. This cell population was then used for further immunophenotyping analysis with specific fluorophores, and gates were based on fluorescence minus one controls, including (1) minus CD11b-VioGreen, (2) minus CD8a-VioBlue, (3) minus CD3e-PE-Vio770, (4) minus CD4-APC, (5) minus anti-NK1.1-PE, (6) minus CD11c-FITC, and (7) minus CD19-APC-Vio770. All data collection and sorting were performed using BD FACS Diva software (BD Biosciences, San Jose, CA, USA), and data analyses were performed using FlowJo software (Tree Star, Ashland, OR, USA). Fluorescence minus one control was used for gating analyses to distinguish positively

from negatively staining cell populations. Compensation was performed using single colour controls.

RNA isolation and qPCR

EVs from WT or engineered HEK293T cells were lysed for RNA isolation using the miRCURY RNA Isolation Kit (Exiqon, Woburn, MA, USA). Frozen tissue samples were homogenised using BeadBlaster (MIDSCI, Valley Park, MO, USA) following three cycles of 6 m/s for 20 s with 30 s pauses between cycles. Total RNA was isolated using the miRNeasy Mini Kit (Qiagen, Valencia, CA, USA) following the manufacturer's protocol, and RNA integrity numbers (RINs) were determined by the Genomics Core Facility at The Ohio State University. miR-199a-3p was quantified as previously described [28] using TaqMan microRNA Assays (Applied Biosystems, Foster City, CA, USA). Data were normalised to the reference genes 18S or U6, and the relative expression was determined using the $2^{-\Delta CT}$ method [39].

Immunohistochemistry

Liver, spleen, and pancreas samples were collected and fixed in 10% neutral buffered formalin for HIS protein detection by the immunohistochemistry test. Paraffin-embedded sections of 10 μm thickness were prepared from these fixed tissue samples and then were deparaffinised and sequentially rehydrated. The immunohistochemistry assay was performed according to the method described by Jia et al. [40]. Primary (rabbit anti-HIS; Cell Signaling Technology, Danvers, MA, USA) and secondary (goat anti-rabbit immunoglobulin G Alexa 488 antibody; Thermo Fisher Scientific, Waltham, MA, USA) antibodies were diluted in blocking buffer with concentrations recommended by the manufacturers. Sections stained with only secondary antibody were used as negative controls. Images were captured using a Zeiss Axio Imager M2.

Statistical analysis

Data were analysed by analysis of variance (ANOVA), followed by pairwise comparisons, with the type I error rate controlled at 0.05. SAS 9.4 statistical software was used for data analysis (SAS, Cary, NC, USA). For Rodent MAP data, values for parameters that were not within the detection threshold were not included in the statistical evaluation.

Results

EV characterisation

Details of EV characterisation data are provided in the supplementary materials section, including (1) the presence of CD63 and TSG101, and the absence of calreticulin in all isolated EVs by Western blot (Supplementary Figure 2a); (2) Cryo-TEM of single EVs (Supplementary Figure 2b); (3) the size distribution and number of EVs by NTA (Supplementary Figure 3); and (4) the presence of miR-199a-3p and 6xHIS protein in Full with 199 EVs by qPCR and Western blot (Supplementary Figure 4).

Immunogenicity evaluation of EVs

Rodent MAP

To determine whether the injected EVs derived from human cell lines would induce an immune response in C57BL/6 mice, 42 cytokines were measured using the Rodent MAP test. Mice challenged with LPS were included as a technical control, and mice receiving vehicle (0.9% saline or PBS with 1% DMSO) were included as negative controls. The results indicated that three injections of LPS elevated the levels of interleukin-18 (IL-18), IL-5, interferon-γ-inducible protein-10 (IP-10), monocyte chemoattractant protein-1 (MCP-1), macrophage-derived chemokine (MDC), macrophage inflammatory protein-1β (MIP-1β), IL-12p40, tissue inhibitor of metalloproteinases-1 (TIMP-1), IL-6, IL-10, plasminogen activator inhibitor-1 (PAI-1), and keratinocyte chemoattractant/growth-regulated oncogene (KC/GRO) compared to saline control (Supplementary Figure 5), which is consistent with the results reported by Jaeger et al. [41]. No significant differences were observed among the five groups (PBS, WT, Empty, Full no 199, and Full with 199) for all 23 antigens that were within detectable ranges, although individual comparisons with the PBS control group did reveal significant differences ($p < 0.05$) for IP-10, MDC, MIP-1β, and vascular cell adhesion molecule-1 (VCAM-1) markers (Table 1)

Spleen cell immunophenotyping

The spleen is the largest lymphoid organ. It plays a critical role in immune responses, and splenocytes are good indicators for initial immunotoxicity screening [42]. To investigate whether EVs would affect the spleen immune cell composition, splenocytes were isolated and the viability was greater than 90% for all the samples. The isolated cells were then stained with surface biomarkers conjugated with different fluorochromes for flow cytometry immunophenotyping experiments. As shown in Figure 1(a, b), there was up-regulation of B-cell surface

Table 1. Cytokine measurement summary for animals treated with extracellular vesicles (n = 10).

Marker	PBS	WT	Empty	Full no 199	Full with 199
IL-5 (pg/mL)	15.5 ± 6.5	22.2 ± 13.5	26.5 ± 12.0	16.0 ± 11.8	24.7 ± 16.5
Insulin (mUI/mL)	135.4 ± 49.4	111.0 ± 51.4	144.4 ± 66.7	112.9 ± 43.5	129.9 ± 34.7
IP-10 (pg/mL)	39.3 ± 12.1	35.2 ± 8.9	45.9 ± 9.9	33.7 ± 7.4*	30.1 ± 7.9*
MCP-1 (pg/mL)	172.8 ± 33.3	188.9 ± 49.6	159.2 ± 53.6	156.0 ± 71.3	179.2 ± 60.0
MDC (pg/mL)	174.5 ± 62.8	171.9 ± 57.0	173.8 ± 70.8	121.2 ± 31.5*	129.8 ± 33.0*
MIP-1β (pg/mL)	17.2 ± 3.5	18.0 ± 3.7	16.6 ± 3.6	14.0 ± 3.0*	13.3 ± 1.7*
SCF (pg/mL)	52.4 ± 15.7	54.4 ± 13.0	55.6 ± 20.9	47.6 ± 3.6	49.8 ± 10.0
VEGF-A (pg/mL)	13.7 ± 2.9	14.0 ± 2.6	13.7 ± 3.6	12.3 ± 1.7	12.5 ± 2.1
CCL6 (ng/mL)	10.5 ± 2.6	9.4 ± 3.3	12.0 ± 2.0	9.5 ± 1.8	10.1 ± 1.2
GCP-2 (ng/mL)	11.7 ± 4.0	12.1 ± 4.6	14.5 ± 2.0	12.5 ± 2.5	14.8 ± 4.3
Eotaxin (pg/mL)	2029 ± 528	1703 ± 745	1571 ± 448	1726 ± 738	1864 ± 491
IL-6 (pg/mL)	15.8 ± 20.1	26.1 ± 32.1	18.1 ± 15.8	14.2 ± 8.3	23.2 ± 17.6
MIP-1α (pg/mL)	226.8 ± 106.2	290.3 ± 121.8	239.5 ± 164.7	143.0[a]	166.6 ± 57.6
RAGE (ng/mL)	2.27 ± 2.43	2.66 ± 1.94	2.04 ± 1.18	3.25 ± 1.39	3.39 ± 3.25
TIMP-1 (ng/mL)	2.36 ± 0.99	2.03 ± 0.74	1.47 ± 0.92	1.41 ± 0.64	1.88 ± 0.85
CRP (μg/mL)	8.71 ± 1.68	9.29 ± 1.48	6.64 ± 1.29	7.63 ± 0.91	7.77 ± 0.98
M-CSF-1 (ng/mL)	1.12 ± 0.34	0.98 ± 0.16	0.92 ± 0.17	0.94 ± 0.11	0.92 ± 0.18
MIP-1γ (ng/mL)	24.4 ± 5.3	21.9 ± 4.6	21.7 ± 4.3	20.5 ± 3.7	20.7 ± 3.0
MMP-9 (ng/mL)	126.5 ± 84.1	110.2 ± 55.4	105.7 ± 41.5	93.8 ± 52.7	181.3 ± 152.1
PAI-1 (ng/mL)	4.93 ± 1.65	5.43 ± 1.57	3.83 ± 1.76	4.20 ± 1.66	5.88 ± 2.31
SAP (μg/mL)	183.6 ± 36.2	194.2 ± 33.6	148.2 ± 22.1	161.9 ± 23.7	164.2 ± 19.3
VCAM-1 (ng/mL)	1692 ± 582	1468 ± 159	1349 ± 285*	1343 ± 97*	1384 ± 145*
KC/GRO (pg/mL)	99.9 ± 86.6	208.3 ± 211.0	130.0 ± 118.9	92.6 ± 90.4	111.5 ± 83.7

Data are shown as mean ± SD. [a]SD is not available owing to the limited data available.

PBS, phosphate-buffered saline control; WT, wild-type HEK293T cells; Empty, HEK293T cells transfected with empty vector; Full no 199, full chimeric construct without miR-199a-3p; Full with 199, full construct with miR-199a-3p; IL, interleukin; IP, interferon-γ-inducible protein; MCP, monocyte chemoattractant protein; MDC, macrophage-derived chemokine; MIP, macrophage inflammatory protein; SCF, stem cell factor; VEGF, vascular endothelial growth factor; CCL, chemokine ligand; GCP, granulocyte chemotactic protein; RAGE, receptor for advanced glycation endproducts; TIMP, tissue inhibitor of metalloproteinases; CRP, C-reactive protein; M-CSF, macrophage colony-stimulating factor; MMP, matrix metalloproteinase; PAI, plasminogen activator inhibitor; SAP, serum amyloid P component; VCAM, vascular cell adhesion molecule; KC/GRO, keratinocyte chemoattractant/growth-regulated oncogene.

*$p < 0.05$ compared to PBS control.

marker CD19 expression in the LPS-positive control group compared to vehicle control. The percentage of B-cell population in the LPS and vehicle control groups was 70.2% and 50.9%, respectively (Figure 1c), suggesting that LPS could induce splenic B-cell proliferation *in vivo*. However, no significant differences were found between the five groups (PBS, WT, Empty, Full no 199, and Full with 199) for any of the tested immune cell populations, indicating that EV treatment did not affect the spleen immune cell composition ($p > 0.05$) (Figure 1d).

General toxicity evaluation

Clinical findings and body weight changes

All 50 mice from the five treatment groups (PBS, WT, Empty, Full no 199, and Full with 199) survived throughout the experimental period, and no animals showed any visible signs of abnormality or behavioural changes. The increase in body weight was normal, and no statistical differences in body weight were observed between the five groups (Table 2).

Haematology and blood chemistry

EV treatment had little effect on the red blood cell, white blood cell, platelet, neutrophil, lymphocyte, and monocyte counts, or on the haematocrit and haemoglobin levels, although there was a significant increase in the percentage of neutrophils for mice in the WT, Empty, and Full groups compared with the PBS control group on day 23 (Table 3). Blood chemistry measurements including albumin, alkaline phosphatase, alanine transaminase, aspartate aminotransferase, blood urea nitrogen, calcium, cholesterol, creatinine, globulin, glucose, and phosphorus are provided in Table 4. No significant difference was observed for any of the tested markers when all five groups were included in the ANOVA.

Gross necropsy and histopathology findings

There were no significant changes in absolute and relative organ weights (data not shown). No gross lesions were identified, including any attributed to EV treatment. Histopathological examination did not reveal any significant abnormalities or treatment-related changes in the full tissue sets examined from mice in any of the treatment groups. Representative photomicrographs of kidney, liver, and spleen from the control and EV treatment groups depict normal histological features (Supplementary Figure 6). All mice in all groups had varying degrees of irregular cytoplasmic vacuolisation of hepatocytes with centralisation of nuclei, consistent with glycogen accumulation (Supplementary Figure 7). Mice were not fasted before being killed, and glycogen levels vary depending on the physiological state of the animal. Virtually all mice

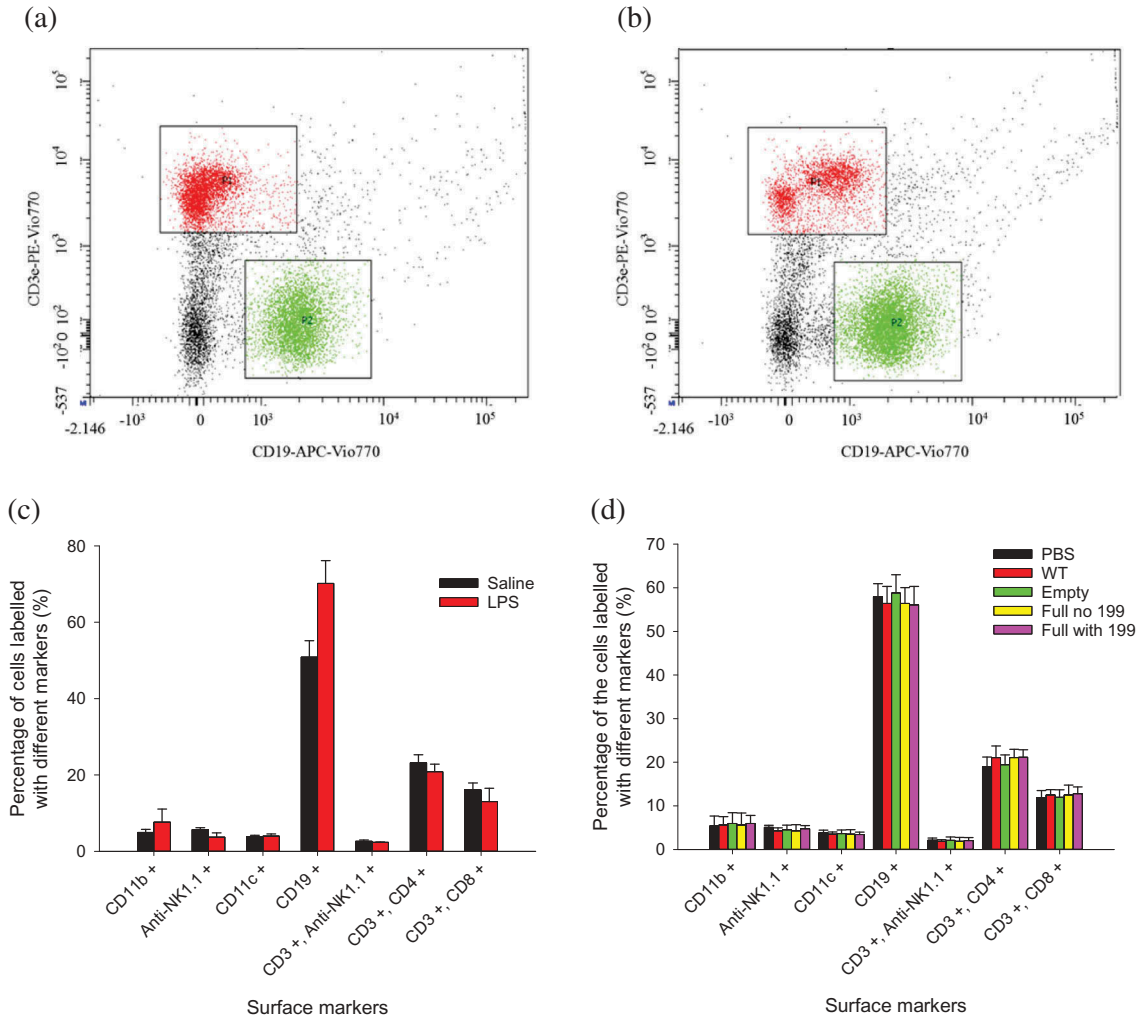

Figure 1. Measurements of different cell populations in spleen cells by flow cytometry using appropriate surface markers conjugated with different fluorochromes. Fluorescence signal of T-cell surface marker CD3e conjugated with PE-Vio770 (P1 = T cells) and B-cell surface marker CD19 conjugated with APC-Vio770 (P2 = B cells) on the cells from mice receiving (a) vehicle control or (b) lipopolysaccharide (LPS). The percentage of each cell population in mice (c) 24 h after LPS treatment (three doses, $n = 4$) or (d) 3 weeks after treatment with extracellular vesicles (10 doses, $n = 10$). Bars and error bars denote the mean and standard deviation, respectively, of experimental groups. PBS, phosphate-buffered saline; WT, wild-type HEK293T cells. *$p < 0.05$.

Table 2. Summary of mouse body weights ($n = 10$).

	Body weight (g)	
Group	Day 1	Day 23
PBS	18.3 ± 0.7	19.5 ± 1.0
WT	18.4 ± 0.8	19.3 ± 0.7
Empty	18.4 ± 0.6	19.7 ± 1.1
Full no 199	18.5 ± 0.8	19.5 ± 0.9
Full with 199	18.6 ± 0.8	19.3 ± 0.6

Data are shown as mean ± SD.
PBS, phosphate-buffered saline control; WT, wild-type HEK293T cells; Empty, HEK293T cells transfected with empty vector; Full no 199, full chimeric construct without miR-199a-3p; Full with 199, full construct with miR-199a-3p.

in all groups also had rare foci of cellular infiltrates randomly distributed in the liver. These infiltrates were typically characterised by necrosis of individual hepatocytes associated with very few inflammatory cells, including neutrophils, lymphocytes, and histiocytes (Supplementary Figure 7). The small number and size of these foci in the liver did not result in altered liver weights or elevations of serum liver enzymes, and therefore were not considered to be clinically significant. Foci of extramedullary haematopoiesis were also occasionally noted in the liver (not shown). Other findings were not indicative of pathology and/or were considered common background lesions in C57BL/6 mice.

Evaluation of EVs in tissues

6xHIS protein detection by immunohistochemistry

To investigate the *in vivo* distribution of the EVs, tissue samples from liver, spleen, and pancreas were

Table 3. Haematology summary for test animals on day 23 (n = 10).

Parameter	PBS	WT	Empty	Full no 199	Full with 199
RBC	10.28 ± 0.43	10.12 ± 0.38	10.31 ± 0.33	10.00 ± 0.42	10.13 ± 0.19
HCT	46.02 ± 1.57	44.99 ± 1.89	46.23 ± 1.17	44.58 ± 1.62	44.78 ± 0.71
HB	15.01 ± 0.49	14.78 ± 0.33	15.19 ± 0.40	14.67 ± 0.39	14.93 ± 0.37
WBC	5.35 ± 1.08	5.62 ± 0.98	4.50 ± 1.30	5.42 ± 1.10	5.04 ± 1.44
NE	0.93 ± 0.22	1.16 ± 0.29	0.99 ± 0.41	1.09 ± 0.33	1.14 ± 0.35
LY	4.18 ± 0.93	4.21 ± 0.74	3.31 ± 0.93	4.07 ± 0.80	3.64 ± 1.05
MO	0.22 ± 0.07	0.22 ± 0.05	0.18 ± 0.08	0.23 ± 0.06	0.23 ± 0.08
NE%	17.58 ± 3.37	20.57 ± 2.88*	21.58 ± 4.83*	19.84 ± 3.22	22.51 ± 2.64*
LY%	77.91 ± 3.20	74.93 ± 2.95	73.62 ± 4.97	75.34 ± 4.37	72.42 ± 2.78
MO%	4.11 ± 0.94	4.01 ± 0.67	4.00 ± 1.31	4.16 ± 0.70	4.59 ± 1.06
PLT	682.6 ± 86.6	663.7 ± 94.5	592.1 ± 174.9	689.6 ± 86.7	696.7 ± 67.1

Data are shown as mean ± SD.

PBS, phosphate-buffered saline control; WT, wild-type HEK293T cells; Empty, HEK293T cells transfected with empty vector; Full no 199, full chimeric construct without miR-199a-3p; Full with 199, full construct with miR-199a-3p; RBC, red blood cell count; HCT, haematocrit; HB, haemoglobin; WBC, white blood cell count; NE, neutrophil count; LY, lymphocyte count; MO, monocyte count; PLT, platelet.

*$p < 0.05$.

Table 4. Blood chemistry summary for test animals (n = 10).

Parameter	PBS	WT	Empty	Full no 199	Full with 199
ALB (g/dL)	3.4 ± 0.2	3.3 ± 0.2	3.4 ± 0.2	3.4 ± 0.1	3.4 ± 0.2
ALP (U/L)	138.5 ± 13.7	142.5 ± 17.0	147.6 ± 17.7	144.3 ± 19.6	129.4 ± 24.3
ALT (U/L)	58.0 ± 28.4	47.2 ± 9.1	49.0 ± 11.9	39.4 ± 10.2	44.4 ± 14.3
AST (U/L)	143.4 ± 46.7	128.9 ± 61.6	137.6 ± 55.8	148.4 ± 71.7	140.1 ± 52.8
BUN (mg/dL)	20.4 ± 2.3	22.6 ± 3.8	24.1 ± 4.8	23.0 ± 4.2	21.0 ± 3.5
CA (mg/dL)	10.7 ± 2.0	10.7 ± 0.7	11.0 ± 0.3	10.9 ± 0.4	11.0 ± 0.5
CHOL (mg/dL)	89.3 ± 8.8	80.9 ± 8.1	84.7 ± 7.2	90.2 ± 10.2	90.2 ± 6.6
CREAT (mg/dL)	0.3 ± 0.05	0.2 ± 0.09	0.3 ± 0.04	0.2 ± 0.06	0.3 ± 0.04
GLOB (U/L)	2.5 ± 0.2	2.4 ± 0.1	2.5 ± 0.4	2.5 ± 0.2	2.5 ± 0.1
GLU (mg/dL)	256.2 ± 60.2	251.1 ± 37.9	252.7 ± 27.3	245.2 ± 32.4	229.6 ± 35.5
PHOS (mg/dL)	11.5 ± 1.8	10.7 ± 2.1	10.4 ± 1.3	11.0 ± 1.5	12.3 ± 1.3
TBILI (mg/dL)	0.3 ± 0.08	0.3 ± 0.08	0.3 ± 0.07	0.3 ± 0.09	0.3 ± 0.09
TPROT (g/dL)	5.9 ± 0.3	5.8 ± 0.3	5.9 ± 0.6	5.9 ± 0.3	6.0 ± 0.2
TRIG (mg/dL)	88.4 ± 18.5	85.4 ± 11.9	88.3 ± 15.9	75.2 ± 8.2	79.7 ± 22.8

Data are shown as mean ± SD.

PBS, phosphate-buffered saline control; WT, wild-type HEK293T cells; Empty, HEK293T cells transfected with empty vector; Full no 199, full chimeric construct without miR-199a-3p; Full with 199, full construct with miR-199a-3p; ALB, albumin; ALP, alkaline phosphatase; ALT, alanine transaminase; AST, aspartate aminotransferase; BUN, blood urea nitrogen; CA, calcium; CHOL, cholesterol; CREAT, creatinine; GLOB, globulin; GLU, glucose; PHOS, phosphorus; TBILI, total bilirubin; TPROT, total protein; TRIG, triglycerides.

collected from PBS control and Full with 199 groups. Tissue were evaluated for the 6xHIS tag protein detection by immunohistochemistry, given the high expression of 6xHIS in the engineered EVs (Supplementary Figure 4b). Expression of 6xHIS protein was present in pancreas from mice receiving Full with 199 EVs (Figure 2). However, no signal was observed in liver or spleen from the same mice, compared to the negative controls (data not shown).

miR-199a-3p quantification by qPCR

To track the disposition of therapeutic EVs, we isolated total RNA from pancreas and liver samples from mice receiving Full with 199 EVs for miR-199a-3p quantification. The RIN for pancreas was too low for qPCR (range 1.0–2.0), but the range for RIN in all liver samples was 7.3–8.7 and these samples were therefore analysed in qPCR. Liver threshold cycle (C_t) values from each sample are presented in Table 5. No significant differences were observed in the livers from the mice receiving Full with 199 EVs compared to the mice receiving PBS (Table 5). Pre-miR-199a-3p was also quantified by qPCR, considering that this part of the RNA contains the modified TAR region and is not present in the mice. C_t values for all the liver samples tested were undetermined, indicating a very low level or an absence of pre-miR-199a-3p.

Discussion

EVs have received increasing interest as therapeutics and as drug carriers. Although their biology is already extensively known, EVs comprise heterogeneous components and may interact with the immune system, causing immunostimulatory or immunosuppressive and potentially toxic effects based on the nature of the donor cells [1,43] and species into which the EVs are being introduced. Therefore, it is crucial to elucidate the immunogenic potential of EVs as they are being tested in preclinical animal models and ultimately in humans.

In this study, we investigated the potential of HEK293T-derived EVs, both WT and engineered, to

Table 5. Threshold cycle (C_t) values of mature miR-199a-3p in liver tissue samples.

Group	Sample ID	miR-199a-3p	U6
PBS	A1	26.4	14.1
	A2	26.4	14.5
	A3	26.4	14.1
	A4	26.5	13.8
Full with 199	E1	26.5	14.2
	E2	26.3	14.2
	E3	26.6	14.5
	E4	26.7	14.7

PBS, phosphate-buffered saline control; Full with 199, full construct with miR-199a-3p.

induce toxicity or to elicit an immune response in C57BL/6 mice. The HEK293T cell line is an immortalised line derived from human embryonic kidney, although its phenotype and molecular characteristics are not typical of renal cells [44]. While it is a non-cancer cell line, HEK293 cells have been demonstrated to grow in immune-compromised mice *in vivo* to form subcutaneous tumours [45]. Furthermore, Li et al. characterised HEK293T-derived EVs by profiling the protein, mRNA, and miRNA components, and they identified some potentially immunogenic molecules at both RNA and protein levels [30]. Therefore, concern has been raised as to whether or not this cell line is safe as a source of therapeutic EVs.

Our results indicate that both WT and engineered EVs obtained from HEK293T cells were overall benign in terms of immune response and toxicity in mice receiving 10 total doses of EVs (8.5 μg protein per dose) over 3 weeks, as no statistically significant differences were observed in any of the markers when evaluated across PBS control and the four EV treatment groups. The LPS-positive control group resulted in up-regulation of B-cell surface biomarker CD19 and increased the percentage of the spleen B-cell population (Figure 2), which is in line with earlier findings [46,47]. Similarly, no significant differences were observed among the five groups for all 23 detectable cytokines (Table 1). However, levels for three of the cytokines tested (IP-10, MDC, and MIP-1β) were significantly lower in the Full no 199 and Full with 199 groups compared to the PBS group, and a fourth cytokine, VCAM-1, was significantly lower in these two groups plus the group dosed with Empty vesicles (EVs obtained from HEK293T cells stably transfected with empty vector). Although WT EVs did not appear to induce any changes in cytokines, the few cytokines that were altered in mice dosed with engineered EVs could suggest that some engineered component, such as the chimeric protein, may have been detected by the mouse's immune system. Overall, these data suggest very limited, if any, immune response of C57BL/6 mice to WT or engineered EVs from HEK293T cells.

Regarding general toxicity, the repeated administration of EVs in mice did not elicit visual signs of toxicity, and no statistical differences in body weight were observed between the five groups (Table 2). The results of complete blood count and blood chemistry panels indicated no significant differenced between the five groups for any of the tested markers (Tables 3 and 4), suggesting no significant effects on haematological and biochemical parameters when evaluated across the five groups. Notably in the haematology analysis, we observed that the WT, Empty and Full with 199 treatment groups demonstrated statistically different (increased) percentage of neutrophils (NE%) compared to the PBS control group in pairwise comparisons, although differences were not present when all treatment groups were included in the ANOVA across all groups, nor were statistical differences found in the absolute neutrophil counts (see Table 3). The histopathological examination of tissues/organs was performed, and no significant gross/histopathological changes were present in the evaluated organs (thymus, heart, lungs, liver, spleen, kidneys, adrenals, ovaries and uterus, and brain), indicating the absence of observable toxicity in the organs (Supplementary Figures 6 and 7).

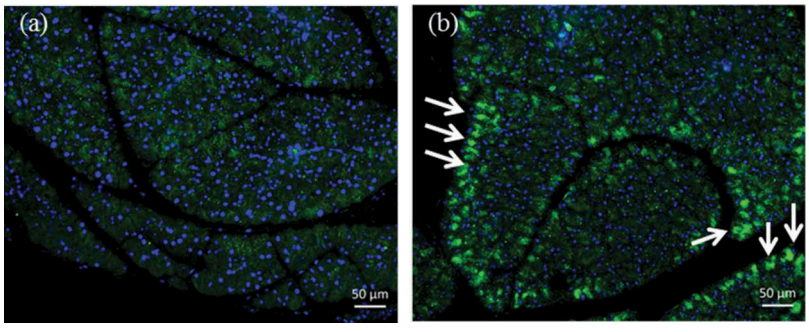

Figure 2. HIS protein detection in pancreas by immunohistochemistry: (a) phosphate-buffered saline control; (b) full construct with miR-199a-3p (Full with 199) extracellular vesicle (EV) treatment group. HIS protein was expressed and detected in the Full with 199 EVs (arrows).

While our study was not specifically designed to track the biodistribution of EVs in mice, we looked for evidence of EV distribution into liver, pancreas, and spleen. We did attempt to follow the biodistribution of the EVs with real-time qPCR focusing on the miR-199 cargo, and we were unable to locate this cargo, which was probably a result of the relatively high background of miR-199 in mouse tissues and the relatively small quantities of cargo being delivered. We also were not able to detect the presence of the 6xHIS tag in liver, although our results do suggest that 6xHIS is present in the pancreas of mice dosed with Full with 199 EVs. It is unclear why we would be able to detect the presence of EVs in pancreas and not in liver, especially since the liver is believed to be a natural scavenger of circulating EVs [48] and since others have demonstrated delivery of HEK293T-derived EVs to the livers of rodents [31]. This may be a function of the timing of tissue collection after the last dose of EVs (24 h after the last intraperitoneal dose and 1 week after the last intravenous dose) and the relative stability of EVs and 6xHIS in liver compared to pancreas. It is also possible that our engineered EVs are not absorbed by the liver to the extent that other EVs have been demonstrated to be absorbed in liver. Wiklander et al. reported that the EV distribution pattern is influenced by the route of administration [31]. In that study, the authors dosed mice with HEK293T-derived EVs by intravenous, intraperitoneal, and subcutaneous routes, and they observed the highest accumulation of EVs in liver, followed by spleen and pancreas after intravenous injection of EVs, but lower EV accumulation in the liver and increased accumulation in the pancreas following intraperitoneal or subcutaneous injection of EVs [31]. Thus, another plausible explanation for our ability to detect EVs in pancreas and not in liver is the frequency of IP dosing within our study.

With respect to the mouse strain used, we chose the C57BL/6 strain of mice because of its wide use for preclinical drug testing and immunology studies [49–51]. At the time these studies were designed and conducted, the dosage of EVs in reported studies had ranged from 1 to 250 μg per injection, and the dosing schedules had varied from one single dose to repeated doses given every other day for 3 weeks [1,35,52–54]. In our study, 8.5 μg (based on protein) of HEK293T-derived EVs were injected in mice three times per week for 3 weeks to provide a total dose of 85 μg protein (see Supplementary Figure 1). While the data suggest that HEK293T cell-derived EVs do not induce an appreciable immune response or toxicity in C57BL/6 mice at the dose level tested, this is only a first look, and several questions remain to be addressed. For example, would higher doses or a longer dosing period produce the same results? What about EVs derived from different cell types? Would human cell-derived EVs be immunogenic or toxic in other mouse strains or in other animal species? While we did not see strong evidence of an immune response based on splenic immune cell populations or circulating cytokine levels, and it is therefore unlikely that immune cell activation is taking place or that anti-drug antibodies are being produced, this should be addressed across multiple studies by investigators utilising different cell types, different dose regimens, and different animal models. Furthermore, it will be important to identify EV-related positive controls that can be used to generate immune responses and toxicities for direct comparison, as our study lacked this type of control. Nonetheless, we hope that the thorough approach taken in our study will provide other investigators with a framework in which to evaluate the immunogenicity and toxicity of their EVs as they work to develop therapeutic EVs in various disease models.

Conclusions

In summary, our results showed that EVs derived from WT and engineered HEK293T cells and dosed at 8.5 μg protein per dose over a 3 week period did not induce either toxicity or an appreciable immune response in immune-competent C57BL/6 mice. Although there have been a few studies published recently investigating the immune response of human EVs in animal models [44,55], this study represents one of the most thorough and extensive investigations into the immunogenicity and toxicity of human cell-derived EVs in mice. These findings highlight the potential application of EVs as drug carriers and will contribute to the various efforts to develop safe EV-based drug-delivery systems.

Acknowledgements

The authors thank the Analytical Cytometry Shared Resource (ACSR), the Comparative Pathology and Mouse Phenotyping Shared Resource (CPMPSR), the Pharmacoanalytical Shared Resource (PhASR), and the Genomics Shared Resource (GSR) within The Ohio State University Comprehensive Cancer Center for technical assistance. The authors thank members of CPMPSR, especially Julie Rectenwald and Jody Sneddon for animal and blood processing, respectively.

Disclosure statement

No potential conflict of interest was reported by the authors.

Funding

This work was supported by the National Center for Advancing Translational Sciences and the National Cancer Institute; NIH grants 1UH2TR000914 and UH3TR000914 to TDS and MAP and P30CA016058.

References

[1] Johnsen KB, Gudbergsson JM, Skov MN, et al. Duroux M. A comprehensive overview of exosomes as drug delivery vehicles - endogenous nanocarriers for targeted cancer therapy. Biochim Biophys Acta. 2014;1846(1):75–87. Epub 2014/04/22.

[2] Vlassov AV, Magdaleno S, Setterquist R, et al. Exosomes: current knowledge of their composition, biological functions, and diagnostic and therapeutic potentials. Biochim Biophys Acta. 2012;1820(7):940–948. Epub 2012/04/17.

[3] Valadi H, Ekstrom K, Bossios A, et al. Exosome-mediated transfer of mRNAs and microRNAs is a novel mechanism of genetic exchange between cells. Nat Cell Biol. 2007;9(6):654–659. Epub 2007/05/09.

[4] Katakowski M, Buller B, Wang X, et al. Functional microRNA is transferred between glioma cells. Cancer Res. 2010;70(21):8259–8263. Epub 2010/09/16.

[5] Mincheva-Nilsson L, Baranov V, Nagaeva O. Isolation and characterization of exosomes from cultures of tissue explants and cell lines. Curr protoc immunol. 2016;115:14 42 1–14 42 21. Epub 2016/11/02.

[6] Greening DW, Xu R, Ji H, et al. A protocol for exosome isolation and characterization: evaluation of ultracentrifugation, density-gradient separation, and immunoaffinity capture methods. Methods mole biol. 2015;1295:179–209. Epub 2015/03/31.

[7] Sun D, Zhuang X, Xiang X, et al. A novel nanoparticle drug delivery system: the anti-inflammatory activity of curcumin is enhanced when encapsulated in exosomes. Mol ther: J Am Soc Gene Ther. 2010;18(9):1606–1614. Epub 2010/06/24.

[8] Wang J, Deng Z, Wang Z, et al. MicroRNA-155 in exosomes secreted from helicobacter pylori infection macrophages immunomodulates inflammatory response. Am J Transl Res. 2016;8(9):3700–3709. Epub 2016/10/12.

[9] Katakowski M, Buller B, Zheng X, et al. Exosomes from marrow stromal cells expressing miR-146b inhibit glioma growth. Cancer Lett. 2013;335(1):201–204. Epub 2013/02/20.

[10] Li L, Piontek K, Ishida M, et al.Extracellular vesicles carry microRNA-195 to intrahepatic cholangiocarcinoma and improve survival in a rat model. Hepatology. 2016. 2017;65(2):501–514.

[11] Lou G, Song X, Yang F, et al. Exosomes derived from miR-122-modified adipose tissue-derived MSCs increase chemosensitivity of hepatocellular carcinoma. J Hematol Oncol. 2015;8:122. Epub 2015/10/31.

[12] Ohno S, Kuroda M. Exosome-mediated targeted delivery of miRNAs. Methods mole biol. 2016;1448:261–270. Epub 2016/06/19.

[13] Bhatnagar S, Shinagawa K, Castellino FJ, et al. Exosomes released from macrophages infected with intracellular pathogens stimulate a proinflammatory response in vitro and in vivo. Blood. 2007;110(9):3234–3244. Epub 2007/08/02.

[14] Bhatnagar S, Schorey JS. Exosomes released from infected macrophages contain Mycobacterium avium glycopeptidolipids and are proinflammatory. J Biol Chem. 2007;282(35):25779–25789. Epub 2007/06/27.

[15] Simhadri VR, Reiners KS, Hansen HP, et al. Dendritic cells release HLA-B-associated transcript-3 positive exosomes to regulate natural killer function. PloS one. 2008;3(10):e3377. Epub 2008/10/15.

[16] Viaud S, Terme M, Flament C. Dendritic cell-derived exosomes promote natural killer cell activation and proliferation: a role for NKG2D ligands and IL-15Ralpha. PloS one. 2009;4(3):e4942. Epub 2009/03/26.

[17] Buschow SI, van Balkom BW, Aalberts M, et al. MHC class II-associated proteins in B-cell exosomes and potential functional implications for exosome biogenesis. Immunol Cell Biol. 2010;88(8):851–856. Epub 2010/05/12.

[18] McLellan AD. Exosome release by primary B cells. Crit Rev Immunol. 2009;29(3):203–217. Epub 2009/06/23.

[19] Zhang H, Xie Y, Li W, et al. CD4(+) T cell-released exosomes inhibit CD8(+) cytotoxic T-lymphocyte responses and antitumor immunity. Cell Mol Immunol. 2011;8(1):23–30. Epub 2011/01/05.

[20] Brennan FR, Morton LD, Spindeldreher S, et al. Safety and immunotoxicity assessment of immunomodulatory monoclonal antibodies. mAbs. 2010;2(3):233–255. Epub 2010/04/28.

[21] Descotes J. Immunotoxicity of monoclonal antibodies. mAbs. 2009;1(2):104–111. Epub 2010/01/12.

[22] McBlane JW. Preclinical safety testing for cell-based products using animals. Biol: J Int Assoc Biol Standardization. 2015;43(5):425–428. Epub 2015/06/01.

[23] Green TM, Alpaugh ML, Barsky SH, et al. Breast cancer-derived extracellular vesicles: characterization and contribution to the metastatic phenotype. Biomed Res Int. 2015;2015:634865. Epub 2015/11/26.

[24] He M, Qin H, Poon TC, et al. Hepatocellular carcinoma-derived exosomes promote motility of immortalized hepatocyte through transfer of oncogenic proteins and RNAs. Carcinogenesis. 2015;36(9):1008–1018. Epub 2015/06/10.

[25] Nakamura K, Sawada K, Kinose Y, et al. Exosomes promote ovarian cancer cell invasion through transfer of CD44 to peritoneal mesothelial cells. Mole cancer res: MCR. 2016. 2017;15(1):78-92.

[26] Pollock K, Stroemer P, Patel S, et al. A conditionally immortal clonal stem cell line from human cortical neuroepithelium for the treatment of ischemic stroke. Exp Neurol. 2006;199(1):143–155. Epub 2006/02/09.

[27] Chen TS, Arslan F, Yin Y, et al. Enabling a robust scalable manufacturing process for therapeutic exosomes through oncogenic immortalization of human ESC-derived MSCs. J Transl Med. 2011;9:47. Epub 2011/04/26.

[28] Chen C, Ridzon DA, Broomer AJ, et al. Real-time quantification of microRNAs by stem-loop RT-PCR. Nucleic Acids Res. 2005;33(20):e179. Epub 2005/11/30.

[29] Martin-Jaular L, de Menezes-Neto A, Monguio-Tortajada M, et al. Corrigendum: Spleen-dependent

immune protection elicited by CpG adjuvanted reticulocyte-derived exosomes from malaria infection is associated with changes in T cell subsets' distribution. Front cell dev biol. 2016;4:153. Epub 2017/01/20.
[30] Li J, Chen X, Yi J, et al. Identification and characterization of 293T cell-derived exosomes by profiling the protein, mRNA and microRNA components. PloS one. 2016;11(9):e0163043. Epub 2016/09/21.
[31] Wiklander OP, Nordin JZ, O'Loughlin A, et al. Extracellular vesicle in vivo biodistribution is determined by cell source, route of administration and targeting. J extracellular vesicles. 2015;4:26316. Epub 2015/04/23.
[32] Kim JH, Badawi M, Park JK, et al. Anti-invasion and anti-migration effects of miR-199a-3p in hepatocellular carcinoma are due in part to targeting CD151. Int J Oncol. 2016;49(5):2037–2045. Epub 2016/10/26.
[33] Lo A, Lin CT, Wu HC. Hepatocellular carcinoma cell-specific peptide ligand for targeted drug delivery. Mol Cancer Ther. 2008;7(3):579–589. Epub 2008/03/19.
[34] Li Y, Hu Y, Xiao J, et al. Investigation of SP94 peptide as a specific probe for hepatocellular carcinoma imaging and therapy. Sci Rep. 2016;6:33511. Epub 2016/09/22.
[35] Alvarez-Erviti L, Seow Y, Yin H, et al. Delivery of siRNA to the mouse brain by systemic injection of targeted exosomes. Nat Biotechnol. 2011;29(4):341–345. Epub 2011/03/23.
[36] Sutaria DS, Jiang J, Elgamal OA, et al. Low active loading of cargo into engineered extracellular vesicles results in inefficient miRNA delivery. J Extracellular Vesicles. Forthcoming 2017.
[37] Rosas LE, Elgamal OA, Mo X, et al. In vitro immunotoxicity assessment of culture-derived extracellular vesicles in human monocytes. J Immunotoxicol. 2016;13(5):652–665. Epub 2016/04/15.
[38] Toomey CB, Cauvi DM, Hamel JC, et al. Cathepsin B regulates the appearance and severity of mercury-induced inflammation and autoimmunity. Toxicol sci: off j Soc Toxicol. 2014;142(2):339–349. Epub 2014/09/23.
[39] Livak KJ. Schmittgen TD. Analysis of relative gene expression data using real-time quantitative PCR and the 2(-Delta Delta C(T)) method. Methods. 2001;25(4):402–408. Epub 2002/02/16.
[40] Jia JZ, Shen YW, Xue AM, et al. Immunohistochemical analysis of cardiac troponin inhibitor in an experimental model of acute myocardial infarction experimental model and in human tissues. Pathol Res Pract. 2015;211(6):456–461. Epub 2015/03/22.
[41] Jaeger LB, Dohgu S, Sultana R, et al. Lipopolysaccharide alters the blood-brain barrier transport of amyloid beta protein: a mechanism for inflammation in the progression of Alzheimer's disease. Brain Behav Immun. 2009;23(4):507–517. Epub 2009/06/03.
[42] Syama S, Gayathri V, Mohanan PV. Assessment of immunotoxicity of dextran coated ferrite nanoparticles in albino mice. Mol Biol Int. 2015;2015:518527. Epub 2015/11/18.
[43] Ha D, Yang N, Nadithe V. Exosomes as therapeutic drug carriers and delivery vehicles across biological membranes: current perspectives and future challenges. Acta pharm Sin B. 2016;6(4):287–296. Epub 2016/07/30.
[44] Martin-Jaular L, de Menezes-Neto A, Monguio-Tortajada M, et al. Spleen-dependent immune protection elicited by CpG adjuvanted reticulocyte-derived exosomes from malaria infection is associated with changes in T cell subsets' distribution. Front cell dev biol. 2016;4:131. Epub 2016/12/03.
[45] Cloutier N, van Eyll O, Janelle ME, et al. Flamand L. Increased tumorigenicity of cells carrying recombinant human herpesvirus 8. Arch Virol. 2008;153(1):93–103. Epub 2007/10/19.
[46] Bucala R. Polyclonal activation of B lymphocytes by lipopolysaccharide requires macrophage-derived interleukin-1. Immunology. 1992;77(4):477–482. Epub 1992/12/01.
[47] Xu H, Liew LN, Kuo IC, et al. The modulatory effects of lipopolysaccharide-stimulated B cells on differential T-cell polarization. Immunology. 2008;125(2):218–228. Epub 2008/03/22.
[48] Imai T, Takahashi Y, Nishikawa M, et al. Macrophage-dependent clearance of systemically administered B16BL6-derived exosomes from the blood circulation in mice. J extracellular vesicles. 2015;4:26238. Epub 2015/02/12.
[49] Yuksel M, Laukens D, Heindryckx F, et al. Hepatitis mouse models: from acute-to-chronic autoimmune hepatitis. Int J Exp Pathol. 2014;95(5):309–320. Epub 2014/08/13.
[50] Dabydeen SA, Furth PA. Genetically engineered ERalpha-positive breast cancer mouse models. Endocr Relat Cancer. 2014;21(3):R195–R208. Epub 2014/02/01.
[51] Scattoni ML, Crawley J, Ricceri L. Ultrasonic vocalizations: a tool for behavioural phenotyping of mouse models of neurodevelopmental disorders. Neurosci Biobehav Rev. 2009;33(4):508–515. Epub 2008/09/06.
[52] Yang Z, Xie J, Zhu J, et al. Functional exosome-mimic for delivery of siRNA to cancer: in vitro and in vivo evaluation. J controlled release: off j Controlled Release Soc. 2016;243:160–171. Epub 2016/11/05.
[53] Qu Z, Wu J, Wu J, et al. Exosomes derived from HCC cells induce sorafenib resistance in hepatocellular carcinoma both in vivo and in vitro. J exp clin cancer res: CR. 2016;35(1):159. Epub 2016/10/08.
[54] Geiger A, Walker A, Nissen E. Human fibrocyte-derived exosomes accelerate wound healing in genetically diabetic mice. Biochem Biophys Res Commun. 2015;467(2):303–309. Epub 2015/10/11.
[55] Tao SC, Yuan T, Rui BY, et al. Exosomes derived from human platelet-rich plasma prevent apoptosis induced by glucocorticoid-associated endoplasmic reticulum stress in rat osteonecrosis of the femoral head via the Akt/Bad/Bcl-2 signal pathway. Theranostics. 2017;7(3):733–750. Epub 2017/03/04.